PAPER Special Section on Wideband Systems

Diversity Reception and Interference Cancellation for Receivers Using Antenna with Periodically Variable Antenna Pattern

Nobuhide KINJO[†], *Nonmember and* **Masato SAITO**[†a)], *Senior Member*

SUMMARY In this paper, we propose a model of a diversity receiver which uses an antenna whose antenna pattern can periodically change. We also propose a minimum mean square error (MMSE) based interference cancellation method of the receiver which, in principle, can suffer from the interference in neighboring frequency bands. Since the antenna pattern changes according to the sum of sinusoidal waveforms with different frequencies, the received signals are received at the carrier frequency and the frequencies shifted from the carrier frequency by the frequency of the sinusoidal waveforms. The proposed diversity scheme combines the components in the frequency domain to maximize the signal-to-noise power ratio (SNR) and to maximize the diversity gain. We confirm that the bit error rate (BER) of the proposed receiver can be improved by increase in the number of arrival paths resulting in obtaining path diversity gain. We also confirm that the proposed MMSE based interference canceller works well when interference signals exist and achieves better BER performances than the conventional diversity receiver with maximum ratio combining.

key words: *space diversity, path diversity, ESPAR antenna, MMSE, interference cancellation*

1. Introduction

Space diversity techniques are effective measures to improve the receiving performance in a multipath fading environment of wireless communications. Although the increase in the number of receive antennas improves receiving performances, the resulting antenna sizes can be a problem because the antennas need separation more than a half wavelength.

To solve the problem, several diversity receivers have been proposed using electronically steerable passive array radiator (ESPAR) antenna whose antenna patterns or directivity would be periodically changed for single-input multiple-output (SIMO) and multiple-input multiple-output (MIMO) receivers [1]–[9]. ESPAR antenna consists of an active element and several parasitic elements [10]. Since the parasitic elements are terminated by variable reactance (VR) elements, we can change the antenna pattern by changing applied voltage to the VR elements. In the previous work mentioned above, they use a sinusoidal voltages to periodically change the antenna pattern in sinusoidal manner. The sinusoidal antenna pattern can generate diversity branches in the frequency domain (See Fig. 1 in Sect. 2).

When we use such an antenna, it is natural to select the amount of frequency-shift (shown as f_s in Fig. 1) so that parts of desired signal is shifted to the frequencies vacant or not used during reception. However, if we fail to find vacant frequencies, the undesired signals may exist at the frequencies to be shifted. In such cases, since both the desired and undesired signals are frequency-shifted by the same amount due to the property of the antenna, they can be interfered with each other (See Fig. 3 in Sect. 3 and Fig. 8 in Sect. 4.2). In this study, we call the undesired signals uniquely caused by periodically variable antenna pattern interfering in the desired signal interference.

Although general array antennas could realize the antenna with periodically variable antenna pattern (PVAP antenna), there are several disadvantages. Firstly, the number of diversity branches built by array antennas is less than that done by ESPAR antennas. Due to the linearity between antenna input and output signals, array antennas are difficult to build useful diversity branches more than the number of antenna elements [11]. On the other hand, ESPAR antennas can construct the number of diversity branches more than the number of antenna elements due to the nonlinear characteristics between the applied voltage to VR elements and antenna patterns [12]. Secondly, it might be difficult to realize high-speed phase switching or have limitation to the speed. Although it depends on the characteristics of VR elements, we experimentally confirmed that ESPAR antennas can change their antenna patterns with more than a hundred MHz [13]. Thirdly, the size of array antennas is relatively larger than that of ESPAR antennas. While array antennas need more than a half wavelength between neighboring antenna elements, the separation between an active element and parasitic elements of ESPAR antennas should be less than a quarter wavelength. Since ESPAR antenna utilizes mutual coupling between antenna elements, the array antenna can be relatively larger size than that of ESPAR antenna. Finally, cabling cost is large in the case of array antennas. The array antennas need the number of cables connecting antenna elements to the receiver is equal to the number of antenna elements. On the other hand, ESPAR antenna only needs one cable which connects the active element and the receiver. Due to the reasons above, ESPAR antennas are the first candidate to realize PVAP antennas.

In this study, we propose a diversity reception scheme for receivers using antenna with periodically variable antenna pattern. Moreover, we study the cases that there exists an interference signal in a frequency-shifted component and there exist multiple interference signals in frequency-shifted components. To reduce the effects from interference signals,

Manuscript received April 10, 2020.
Manuscript revised August 7, 2020.

[†]The authors are with University of the Ryukyus, Okinawa-ken, 903-0213 Japan.
a) E-mail: masato_saito@m.ieice.org

DOI: 10.1587/transfun.2020WBP0006

we propose a minimum mean square error (MMSE) based interference cancellation method.

Numerical results confirm that the proposed the proposed receiver, whose antenna size is less than that of two-element array antenna, achieves similar bit error rate (BER) to that obtained by the receiver with three-element array antenna and maximum ratio combining (MRC) when the number of received paths is sufficiently large. Therefore, the receiver can achieve path diversity gain. Also, we confirm that the proposed MMSE based interference canceller can reduce the interference effectively for both cases of existing a single and double interference signals in the neighboring frequency bands.

This paper is organized as following. In Sect. 2, the system model is illustrated. Section 3 explains the proposed diversity receiver and interference canceller. Then, in Sect. 4, numerical results obtained by computer simulation are provided to evaluate the BER performances obtained by the proposed receiver. Finally, Sect. 5 concludes this study.

2. System Model

In this section, first, we describe the receiving process of the receiver with an antenna with periodically variable antenna pattern (PVAP antenna). Then, we propose a system model of the diversity receiver with PVAP antenna. The PVAP antenna can be realized by ESPAR antenna [1], [6], [8], [14]. In general, ESPAR antenna consists of an active antenna element and multiple passive antenna elements. The passive elements are terminated by VR elements [10], [15]. To the multiple VR elements, if we apply a combination of constant voltages, we can arrange the antenna beam pattern according to the combination [10]. Instead of those constant voltages, periodical voltages, for example, sinusoidal voltages can be applied to the elements in order to change the antenna pattern in a periodic manner [8], [16], [17].

In this study, we focus on periodically varying the antenna patterns of ESPAR antennas. We build a time-variable antenna pattern model of the PVAP antenna. The ESPAR antenna considered here has N_{pe} parasitic elements. Suppose that we apply the following DC biased sinusoidal voltage to the VR element of the k-th parasitic element of the antenna for $k = 1, \ldots, N_{\mathrm{pe}}$.

$$v_k(t) = V_{0,k} + V_{1,k} \cos(\omega_{\mathrm{s}} t + \theta_{0,k}) \tag{1}$$

where $V_{0,k}$ is DC voltage, $V_{1,k}$ is the amplitude of sinusoidal component, ω_{s} is an angular frequency common to all the VR elements, and $\theta_{0,k}$ is the initial phase of the sinusoidal component. The voltages can change the reactance of each parasitic element, then the change of reactance can vary the antenna pattern or directivity of the antenna. Since the relation between applied voltage waveforms and the obtained antenna patterns are nonlinear, the antenna patterns can have harmonic components of ω_{s}. However, we found experimentally that such harmonics could be relatively weak compared with the components of DC and the fundamental frequencies $\pm\omega_{\mathrm{s}}$ [16]. Therefore, we assume the following antenna pattern generated by the waveforms (1) without harmonic components for a given azimuth ϕ and time t.

$$D(\phi, t) = D_{-1}(\phi)\, \mathrm{e}^{-j\omega_{\mathrm{s}} t} + D_0(\phi) + D_1(\phi)\, \mathrm{e}^{j\omega_{\mathrm{s}} t} \tag{2}$$

where $D_{-1}(\phi)$, $D_0(\phi)$, and $D_1(\phi)$ are complex Fourier coefficients of $D(\phi, t)$ corresponding to the frequencies of $-\omega_s$, 0 (DC), and ω_s, respectively. In this study, we consider only the azimuth angle as the direction of arrival path for simplicity. However, it is straightforward to generalize it to azimuth and elevation angles. Note that the actual coefficients can be determined by the structure of the antenna, the characteristics of VR elements, applied waveforms (1), azimuth, and so forth.

When a receive antenna receives a signal from a direction, the antenna output can be mathematically shown as the product of the received signal and the antenna pattern for the direction. Suppose that a signal coming from a direction ϕ can be given as $r(\phi, t)$. If we use the antenna whose antenna pattern is given by (2), the baseband antenna output $y(\phi, t)$ can be shown as follows.

$$\begin{aligned} y(\phi, t) &= r(\phi, t)\, D(\phi, t) && (3)\\ &= r(\phi, t)\, D_{-1}(\phi)\, \mathrm{e}^{-j\omega_{\mathrm{s}} t} \\ &\quad + r(\phi, t)\, D_0(\phi) \\ &\quad + r(\phi, t)\, D_1(\phi)\, \mathrm{e}^{j\omega_{\mathrm{s}} t}. && (4) \end{aligned}$$

In the right-hand member of (4), each term can be orthogonal to each other, if ω_s is sufficiently large. Hereafter, we assume that ω_s is large enough to keep the orthogonality between the received signal components in the frequency region. Considering the orthogonality, we can write (4) in the following equivalent vector form.

$$\begin{bmatrix} y_{-1}(\phi, t) \\ y_0(\phi, t) \\ y_1(\phi, t) \end{bmatrix} = \begin{bmatrix} D_{-1}(\phi) \\ D_0(\phi) \\ D_1(\phi) \end{bmatrix} r(\phi, t) \tag{5}$$

where $y_k(\phi, t)$ for $k = -1, 0, 1$ are the received signal components at the frequencies of $k\omega_{\mathrm{s}}$. We define N_{r} as the number of orthogonal components of the received signals (5). The number can be also recognized as the number of receive diversity branches. In the case of (5), $N_{\mathrm{r}} = 3$.

In multipath fading environments, received signals or elementary waves could come from multiple directions. Therefore, when N_{p} signals from the directions of ϕ_k for $k = 1, \ldots, N_{\mathrm{p}}$ arrive at the receiver, the antenna output in the vector form can be shown as

$$\begin{aligned} \boldsymbol{y} &= \begin{bmatrix} y_{-1}(t) \\ y_0(t) \\ y_1(t) \end{bmatrix} = \sum_{k=1}^{N_{\mathrm{p}}} \begin{bmatrix} D_{-1}(\phi_k) \\ D_0(\phi_k) \\ D_1(\phi_k) \end{bmatrix} r(\phi_k, t) && (6)\\ &= D\boldsymbol{r}, && (7) \end{aligned}$$

where D is the $N_{\mathrm{r}} \times N_{\mathrm{p}}$ matrix including antenna pattern coefficients which is given as

$$D = \begin{bmatrix} D_{-1}(\phi_1) & D_{-1}(\phi_2) & \cdots & D_{-1}\left(\phi_{N_{\mathrm{p}}}\right) \\ D_0(\phi_1) & D_0(\phi_2) & \cdots & D_0\left(\phi_{N_{\mathrm{p}}}\right) \\ D_1(\phi_1) & D_1(\phi_2) & \cdots & D_1\left(\phi_{N_{\mathrm{p}}}\right) \end{bmatrix}, \tag{8}$$

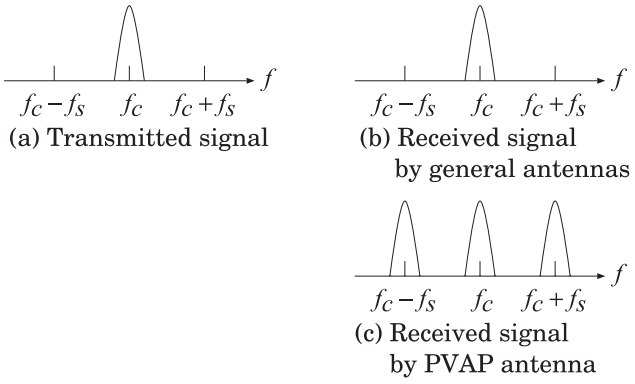

Fig. 1 Spectra of (a) transmitted signal or input signal to the received antenna, (b) received signal received by general antennas, and (c) received signal received by PVAP antenna.

and $\boldsymbol{r}$ is the vector of received signals shown as

$$\boldsymbol{r} = \left[r(\phi_1, t) \quad r(\phi_2, t) \quad \cdots \quad r\left(\phi_{N_\mathrm{p}}, t\right) \right]^\mathrm{T}, \tag{9}$$

where $^\mathrm{T}$ is a transpose operator. Hereafter, we refer to D and $\boldsymbol{r}$ as antenna pattern matrix and received signal vector, respectively. As a visualized reference, in Fig. 1, we illustrate the spectra of (a) a transmitted signal or equivalently an input signal to the received antennas, (b) a received signal received by general antennas, and (c) a received signal received by the PVAP antenna whose antenna patterns are given in (2). Here, we assume the carrier frequency of the transmitted signal is f_c as shown in Fig. 1(a). As shown in Fig. 1(c), the antenna pattern generates three received signal components in the frequency domain at the frequencies $f_\mathrm{c} - f_\mathrm{s}$, f_c, and $f_\mathrm{c} + f_\mathrm{s}$, where $f_\mathrm{s} = \omega_\mathrm{s}/2\pi$. After frequency conversion to baseband, the components at $f_\mathrm{c} - f_\mathrm{s}$, f_c, and $f_\mathrm{c} + f_\mathrm{s}$ in Fig. 1(c) can be written as (7).

Instead of (1), if we consider a DC component and $(N_\mathrm{r}-1)/2$ orthogonal sinusoidal voltages, we can generalize the antenna pattern as

$$D(\phi, t) = \sum_{k=-(N_\mathrm{r}-1)/2}^{(N_\mathrm{r}-1)/2} D_k(\phi)\, \mathrm{e}^{jk\omega_\mathrm{s}t}. \tag{10}$$

As with the case of $N_r = 3$ shown in (2), we assume that for a given number of orthogonal sinusoidal voltages the effects of harmonic components can be ignored to generate only N_r orthogonal components as shown in (10). Then, the corresponding antenna pattern matrix to (10) is given for N_p arrival paths as

$$D = \begin{bmatrix} D_{-(N_\mathrm{r}-1)/2}(\phi_1) & \cdots & D_{-(N_\mathrm{r}-1)/2}\left(\phi_{N_\mathrm{p}}\right) \\ \vdots & \ddots & \vdots \\ D_0(\phi_1) & \cdots & D_0\left(\phi_{N_\mathrm{p}}\right) \\ \vdots & \ddots & \vdots \\ D_{(N_\mathrm{r}-1)/2}(\phi_1) & \cdots & D_{(N_\mathrm{r}-1)/2}\left(\phi_{N_\mathrm{p}}\right) \end{bmatrix}. \tag{11}$$

Since the symmetry of the frequencies $k\omega_\mathrm{s}$, N_r should be an odd number.

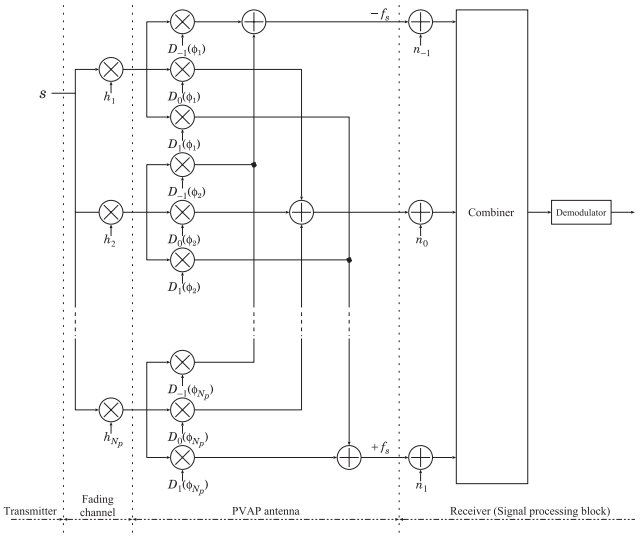

Fig. 2 System model including the receiver with PVAP antenna ($N_\mathrm{r} = 3$).

Based on the receiving process mentioned above, we describe the system model of the receiver with PVAP antennas. The proposed model is shown in Fig. 2. The transmitter sends a complex symbol s to the receiver through multipath fading channel. The average power of s is assumed $\mathrm{E}\left[|s|^2\right] = 1$, where $\mathrm{E}[\cdot]$ is an averaging operator giving the average value of the argument. The carrier frequency is f_c.

The number of arrival paths at the receive antenna is N_p. Each path experiences fading effects, then the path coming from a direction ϕ_k is multiplied by a complex channel coefficient h_k. Since we assume Rayleigh fading channel throughout this paper, the coefficient h_k can be a complex Gaussian random variable with the mean $\mathrm{E}[h_k] = 0$ and the mean square $\mathrm{E}\left[|h_k|^2\right] = 1$.

The arrival signal coming from the direction ϕ_k can be shown as

$$r_k = h_k s. \tag{12}$$

When N_p paths arrive at the antenna, all the arrival paths can be given in a vector form as

$$\boldsymbol{r} = \boldsymbol{h} s, \tag{13}$$

where $\boldsymbol{h}$ is a vector of channel coefficients and is defined as

$$\boldsymbol{h} = \left[h_1 \quad h_2 \quad \cdots \quad h_{N_\mathrm{p}} \right]^\mathrm{T}. \tag{14}$$

Note that the carrier frequency of each path in (13) is f_c but not $f_\mathrm{c} \pm f_\mathrm{s}$. As shown in Fig. 2, the components at $f_\mathrm{c} \pm f_\mathrm{s}$ are generated inside the antenna but not during propagation.

Substituting (13) into (7) and considering additive white Gaussian noise (AWGN) in the channel, we have the antenna outputs in a vector form $\boldsymbol{y} \in \mathbb{C}^{N_\mathrm{r} \times 1}$ as

$$\boldsymbol{y} = D\boldsymbol{r} + \boldsymbol{n} = D\boldsymbol{h}s + \boldsymbol{n} \tag{15}$$

where $\boldsymbol{n} \in \mathbb{C}^{N_\mathrm{r} \times 1}$ is the noise vector defined as

$$\boldsymbol{n} = \left[n_{-(N_r-1)/2} \quad \cdots \quad n_0 \quad \cdots \quad n_{(N_r-1)/2} \right]^{\mathrm{T}}. \tag{16}$$

Here, we assume the component of (16) has zero mean $\mathrm{E}[n_k] = 0$ and the variance $\mathrm{E}\left[|n_k|^2\right] = 2\sigma^2$. Then, N_r antenna outputs are divided into N_r separated branches in the frequency domain as shown in Figs. 1 and 2 for the case $N_r = 3$. Each component of $\boldsymbol{y}$ is transferred into a combiner. The combiner gives an output as a decision variable for a demodulator.

3. Proposed Method

In this section, we propose a diversity receiver with the PVAP antenna. Then, we consider the case of existing interference signals in the neighboring frequencies. After that we propose an interference canceler for the receiver based on MMSE criteria.

First, we discuss the behavior of the interference signals when PVAP antenna is used at the receiver. The spectra of the received signals, which are desired and interference, are shown in Fig. 3. Figure 3(a) and Fig. 3(b) show the spectra of the antenna inputs and outputs, respectively. Here, the carrier frequency of the desired signal is f_c. As is the case in Fig. 1, the desired signal can be frequency-shifted by $\pm f_s$ according to the antenna property and appeared at not only f_c, but also $f_c \pm f_s$, as shown in Fig. 3(b). When the carrier frequencies of $f_c - f_s$ and $f_c + f_s$ are used by other transmitters, their transmitted signals can be interference signals. If two interference signals are sent with their carrier frequencies of $f_c \pm f_s$, the received signals also suffer from the antenna property. Therefore, the property makes the desired as well as interference signals frequency-shift by $\pm f_s$. As can be seen from Fig. 3(b), any signal appears at its carrier frequency as well as its neighboring frequencies due to the property of PVAP antenna. Therefore, if there are interference signals at either or both of $f_c - f_s$ and $f_c + f_s$, the desired signal components at f_c and $f_c \pm f_s$ suffer from the interference.

Then, we describe the system model of the proposed diversity receiver with interference signals. The system model is shown for the number of arrival paths $N_p = 2$ and the number of diversity branches $N_r = 3$ in Fig. 4.

We assume that the carrier frequencies of the desired signal s_0 is f_c. We also assume two interference signals s_{-1} and s_1 are centered at $f_c - f_s$ and $f_c + f_s$, respectively. The receiver can select ω_s. It is natural to avoid interference signals when selecting the angular frequency ω_s. However, here, we consider a relatively severe case for receiving desired signal in terms of interference. The power of signals are normalized as $\mathrm{E}\left[|s_k|^2\right] = 1$ for $k = -1, 0, 1$. Using the receiving process discussed in the previous section, we have the antenna outputs $\boldsymbol{y}$ in the vector form as

$$\boldsymbol{y} = D_{-1}\boldsymbol{h}_{-1}\frac{s_{-1}}{\sqrt{\gamma_{-1}}} + D_0\boldsymbol{h}_0 s_0 + D_1\boldsymbol{h}_1\frac{s_1}{\sqrt{\gamma_1}} + \boldsymbol{n}, \tag{17}$$

where γ_k for $(k = -1, 1)$ is signal-to-interference power ratio (SIR), the power ratio of the desired signal to the interference signals at $f_c + kf_s$, $\boldsymbol{h}_k$ and D_k are the channel coefficients vector and the antenna pattern matrix for s_k, respectively. The channel coefficients vector $\boldsymbol{h}_k$ is given as

$$\boldsymbol{h}_k = \left[h_{1,k} \quad h_{2,k} \quad h_{N_p,k} \right]^{\mathrm{T}}. \tag{18}$$

Considering the overlap between signals (see Fig. 3(b)), we can write the antenna matrices D_{-1}, D_0, and D_1 as

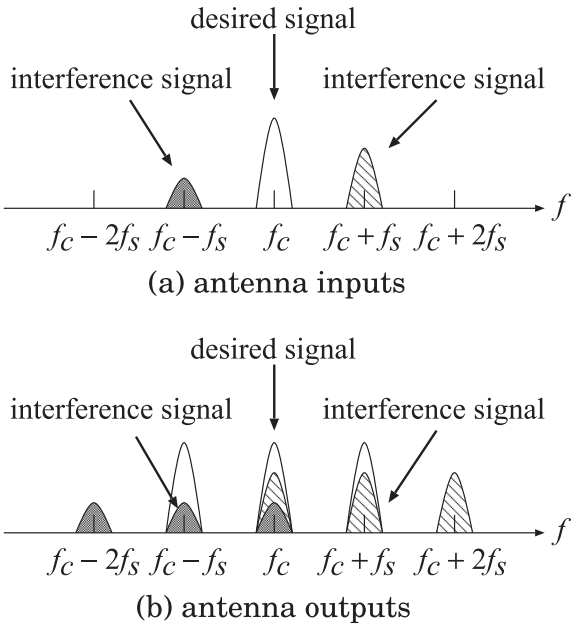

Fig. 3 Spectra of received signals at the antenna inputs and outputs with interference signals in the neighboring frequencies.

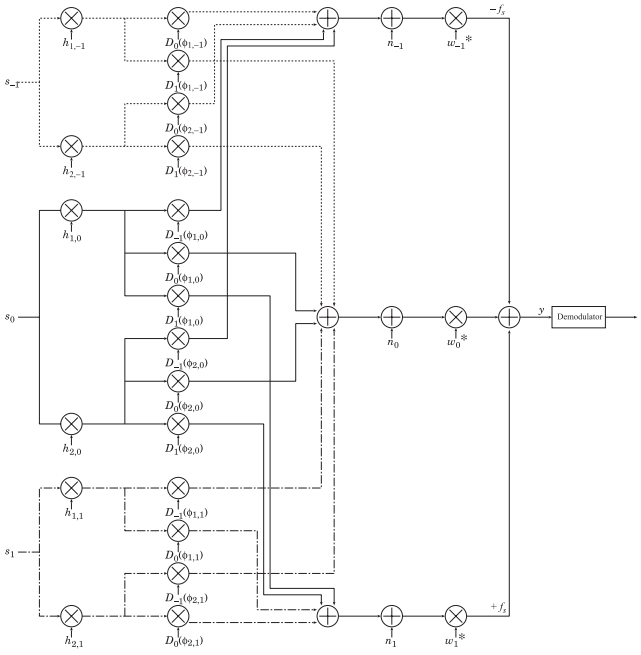

Fig. 4 System model of the proposed diversity receiver with interference signals ($N_p = 2$, $N_r = 3$).

$$D_{-1} = \begin{bmatrix} D_0(\phi_{1,-1}) & \cdots & D_0(\phi_{N_p,-1}) \\ D_1(\phi_{1,-1}) & \cdots & D_1(\phi_{N_p,-1}) \\ 0 & \cdots & 0 \end{bmatrix}, \tag{19}$$

$$D_0 = \begin{bmatrix} D_{-1}(\phi_{1,0}) & \cdots & D_{-1}(\phi_{N_p,0}) \\ D_0(\phi_{1,0}) & \cdots & D_0(\phi_{N_p,0}) \\ D_1(\phi_{1,0}) & \cdots & D_1(\phi_{N_p,0}) \end{bmatrix}, \tag{20}$$

and

$$D_1 = \begin{bmatrix} 0 & \cdots & 0 \\ D_{-1}(\phi_{1,1}) & \cdots & D_{-1}(\phi_{N_p,1}) \\ D_0(\phi_{1,1}) & \cdots & D_0(\phi_{N_p,1}) \end{bmatrix}, \tag{21}$$

respectively. The third row of (19) corresponds to the antenna pattern coefficients for the frequency band centered at $f_c - 2f_s$. Since the frequency band should not include the desired signals in this model, we set zeros the row to ignore the components in the frequency band. For the same reason, the first row of (21) is also a zero vector.

The antenna output (17) is multiplied by the Hermitian transpose of a weight vector $\boldsymbol{w} \in \mathbb{C}^{N_r \times 1}$. The weight vector $\boldsymbol{w}$ is given as

$$\boldsymbol{w} = \begin{bmatrix} w_{-1} & w_0 & w_1 \end{bmatrix}. \tag{22}$$

In Fig. 4, * means a complex conjugate operator. Hence, the decision variable z for demodulation can be given as

$$z = \boldsymbol{w}^{\mathrm{H}} \boldsymbol{y}, \tag{23}$$

where $^{\mathrm{H}}$ is a Hermitian transpose operator. In this study, we determine the weight vector $\boldsymbol{w}$ according to MMSE criteria [18]. We define an objective function J as the mean square error between the decision variable z and the desired signal s_0 [19]. Then, the function J is given as

$$J = \mathrm{E}\left[|z - s_0|^2\right] \tag{24}$$

$$= \mathrm{E}\left[\left|\boldsymbol{w}^{\mathrm{H}} \boldsymbol{y} - s_0\right|^2\right]. \tag{25}$$

The weight vector $\boldsymbol{w}$ which minimizes (25) can be obtained through a mathematical manipulation given in Appendix in detail, as

$$\boldsymbol{w} = \left(\frac{1}{\gamma_{-1}} R_{-1} + R_0 + \frac{1}{\gamma_1} R_1 + 2\sigma^2 I_{N_r}\right)^{-1} \mathrm{E}\left[D_0 \boldsymbol{h}_0\right]. \tag{26}$$

where R_i is the autocorrelation matrix of the vector $D_i \boldsymbol{h}_i$, we refer to this vector as equivalent channel vector, $1/2\sigma^2$ means signal-to-noise power ratio (SNR)[†] because $\mathrm{E}\left[|s_0|^2\right] = 1$, and I_{N_r} is the identity matrix whose size is $N_r \times N_r$. The autocorrelation matrix is given as follows.

$$R_k = \mathrm{E}\left[(D_k \boldsymbol{h}_k)(D_k \boldsymbol{h}_k)^{\mathrm{H}}\right]. \tag{27}$$

[†]Since the noise variance is for each diversity branch here, this definition of SNR means the SNR per diversity branch. When we consider the SNR of the ratio of the total received power arrived at the receiver to the total noise variance, we need to replace $2\sigma^2$ in (26) to $2\sigma^2/N_r$. Besides, the total antenna gain should be normalized to 1 in (31).

4. Numerical Results

In this section, we show BER performances of the system with the proposed diversity receiver in the cases of both without and with interference signals. As the modulation scheme of the transmitted symbol, we use binary phase shift keying (BPSK). That is, $s_0 \in \{-1, +1\}$. For comparison purpose, we use the theoretical BER of BPSK signaling in Rayleigh fading channel using the diversity receiver with MRC, which is shown as "MRC theory" in the following figures, as a case of a conventional diversity receiver shown as [20]–[22]

$$\overline{P_{e,\mathrm{MRC}}^{(L)}(\Gamma)} = \left(\frac{1-\alpha}{2}\right)^L \cdot \sum_{k=0}^{L-1} \binom{L-1+k}{k} \left(\frac{1+\alpha}{2}\right)^k \tag{28}$$

where Γ is the average SNR, L is the number of diversity branches, and α is given as

$$\alpha = \sqrt{\frac{\Gamma}{1+\Gamma}}. \tag{29}$$

When the number of diversity branches is L, the receiver with MRC requires L antenna elements which are separated by more than a half wavelength.

4.1 BER Performances (without Interference)

First we evaluate BER performances of the system with the proposed diversity receiver using the system model shown in Fig. 2. In this case, we consider the system without interference. The parameter setting for the simulation is tabulated in Table 1. As for the antenna size, we assume the following things for both ESPAR antennas and array antennas. ESPAR antennas requires 2 to 6 parasitic elements located circularly around an active element with the distance of one-eighth wavelength or $\lambda/8$ [8], [23]. Thus, the size of diameter of the ESPAR antenna is $\lambda/4$. For array antennas, since at least a half wavelength is required between neighboring antenna elements, for $L = 2, 3, 5, 7$ the sizes of the linear array antenna become $\lambda/2$, λ, 2λ, and 3λ, respectively. Thus, ESPAR antenna can reduce the antenna sizes compared with array antennas with two elements. Of course, precise comparison of antenna sizes requires more detailed configurations of both antennas and further studies on PVAP antennas. However, since the studies are beyond our scope, we remain the precise comparison of antenna sizes as future work.

As for the antenna pattern coefficients for a direction ϕ in (10), we assume that the ratio of antenna pattern gain of the DC component to the other components satisfy the following conditions.

Table 1 Simulation parameters used in Sect. 4.1.

Parameter	Value, Method
Modulation scheme	BPSK
The number of paths N_p	2, 8, 16
The number of diversity branches N_r	3, 5, 7
Gain ratio ρ (30) [dB]	0, 8, 12, 20, 50
Channel	Raleigh fading + AWGN
Combining method	MRC

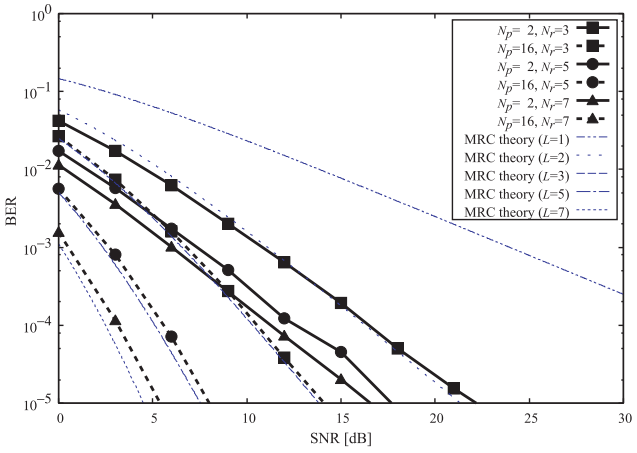

Fig. 5 BER performances obtained by the proposed diversity receiver for various N_p and N_r.

$$\rho = \frac{|D_0(\phi)|^2}{|D_k(\phi)|^2} = \text{const.} \tag{30}$$

for $k = -(N_\mathrm{r}-1)/2, \ldots, -1, 1, \ldots, (N_\mathrm{r}-1)/2$. When N_p paths arrive, the coefficients are normalized as

$$\sum_{k=-(N_\mathrm{r}-1)/2}^{(N_\mathrm{r}-1)/2} \sum_{l=1}^{N_\mathrm{p}} |D_k(\phi_l)|^2 = N_\mathrm{r}. \tag{31}$$

Since we consider SNR per branch as mentioned in the previous section, the total gain of the antenna pattern coefficients is normalize to N_r. If $|D_k(\phi_l)|^2$ for all k and l are equivalent to each other, the constraint (31) makes the power of coefficients $|D_k(\phi_l)|^2 = 1/N_\mathrm{p}$. The assumptions (30) and (31) are to normalize the autocorrelation matrices of equivalent channel vectors. We also assume that the phase of the coefficients $D_k(\phi_l)$ are uniform random variables in the range $[0, 2\pi)$.

The BER performances of the system using the proposed diversity antenna versus SNR are shown for different values of diversity branches $N_\mathrm{r} = 3$, 5, and 7 and $\rho = 1$ in Fig. 5. In the figure, black solid lines show BER for $N_\mathrm{p} = 2$, i.e., smaller number of arrival paths, while black dotted lines for $N_\mathrm{p} = 16$, i.e., in a relatively multipath rich environment. In addition, blue lines mean theoretical BER performances using MRC for the number of diversity branches $L = 1$, 2, 3, 5, and 7 obtained by (28). From the figure, we find three facts. Firstly, by the proposed receiver, BER performances can be improved when N_p increases. Hence, the proposed receiver gains more in multipath rich environments. Secondly, for a large number of arrival paths N_p, the BER performances for N_r branches approach to those for MRC using L equivalent to N_r. This result implies that, in the environment of large N_p, even the proposed receiver with N_r branches is smaller in size compared with the conventional diversity receiver, it can obtain almost the same diversity gain as the conventional diversity receiver with MRC of L antenna elements. Based on these findings, the proposed diversity technique can be categorized into path diversity. Lastly, increasing N_r improves the diversity order, that is, the slopes of BER curves become steeper when N_r is increased from 3 to 7.

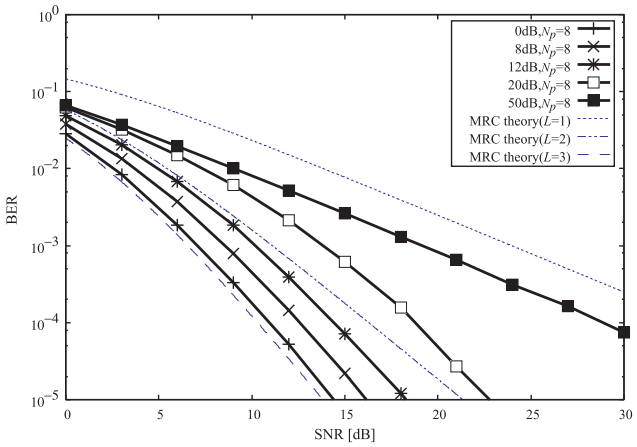

Fig. 6 BER performances obtained by the proposed diversity receiver with antenna gain difference ($N_\mathrm{r} = 3, N_\mathrm{p} = 8$).

In the actual antenna, the gain of antenna patterns for DC component tend to be larger than those for frequency-shifted components [24]. Thus, we evaluate the performances in existing the gain differences. We consider the case that the ratio $\rho > 1$ or $|D_k(\phi_l)|^2 < |D_0(\phi_l)|^2$ for $k \neq 0$. In the following numerical results, we use the ratio $|D_0(\phi_l)|^2 / |D_k(\phi_l)|^2$ as a parameter to indicate antenna gain difference. We assume for a given direction ϕ

$$|D_k(\phi)|^2 = |D_l(\phi)|^2 \tag{32}$$

for $k \neq l$, $k \neq 0$, and $l \neq 0$. Thus, the gains for frequency-shifted components are equivalent to each other.

The BER performances in the case of existing gain differences between diversity branches are shown for $N_\mathrm{r} = 3$ and $N_\mathrm{p} = 8$ in Fig. 6. From the figure, we can see that diversity gain decreases with increasing the gain difference. Therefore, the antenna gain for each direction and each frequency-shifted component should be equivalent to each other to minimize BER. If the gain difference is less than 12 dB, we can obtain equivalent diversity gain, which is shown as the slope of the curves, to that of the conventional diversity receiver with $L = 3$. In addition, in the case of the gain difference, it can be also achieved better BER performances than those of the conventional one with $L = 2$.

We shall add the performance evaluations considering antenna configurations. In a configuration of ESPAR antennas, the phase of antenna pattern coefficients cannot

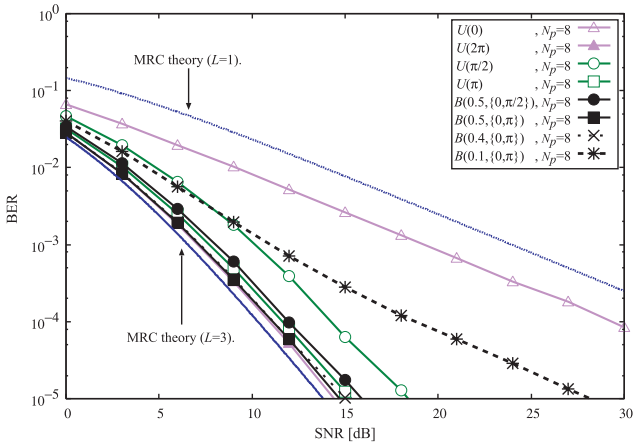

Fig. 7 BER performances obtained by the proposed diversity receiver for various phase distributions of antenna pattern coefficients ($N_r = 3, N_p = 8$) [25].

be approximated to uniform random variables in the range $[0, 2\pi)$ [24]. Thus, it might be interesting to observe the degradation of BER performances due to statistical characteristics of the phases of the coefficients [25]. The knowledge may help designers in designing the antenna. In this paper, we consider two kinds of distributions, uniform and Bernoulli distributions, as the statistical model of the phase of antenna pattern coefficients $D_k(\phi)$ based on the previous work on antenna designing [24]. As notations, we use

- $U(\theta_{\max})$: Uniform distribution in the range of $[0, \theta_{\max}]$.
- $B(p, \{\theta_0, \theta_1\})$: Bernoulli distribution with the probabilities $P(\theta_0) = p$ and $P(\theta_1) = 1 - p$.

The BER performances based on the statistical phase models are shown in Fig. 7. We show the cases of $U(0)$, $U(\pi/2)$, $U(\pi)$, and $U(2\pi)$ for uniform distribution and $B(0.1, \{0, \pi\})$, $B(0.4, \{0, \pi\})$, $B(0.5, \{0, \pi\})$, $B(0.5, \{0, \pi/2\})$ for Bernoulli distributions. Here, $U(0)$ corresponds to the use of omnidirectional antennas in terms of both gain and phase. As we can see from the figure, when the phase distribution is $U(0)$, any path diversity gain cannot be obtained. However, when we compare $U(0)$ and SISO, which is labeled as MRC theory ($L = 1$), some gain can be obtained due to multiple diversity branches ($N_r = 3$).

If the phase distributions are $U(\pi/2)$, $U(\pi)$, and $U(2\pi)$, the equivalent diversity gain to the conventional diversity with $L = 3$ is achieved. Wider distribution range gains more, and the phase distribution range $\theta_{\max} > \pi$ is sufficient to achieved BER performance close to that of the conventional diversity with $L = 3$.

When the distribution is Bernoulli distributions $B(0.4, \{0, \pi\})$, $B(0.5, \{0, \pi\})$, $B(0.5, \{0, \pi/2\})$, BER performances close to the case of $U(2\pi)$ can be obtained. It is relatively weak effects of difference between two phases of Bernoulli distributions on BER performances. On the other hand, the difference of a priori probabilities impacts on the performances when we compare the performances between $B(0.1, \{0, \pi\})$ and $B(0.5, \{0, \pi\})$.

Table 2 Simulation parameters used in Sect. 4.2.

Parameter	Value, Method
Modulation scheme	BPSK
The number of paths N_p	2, 4, 8, 16
The number of diversity branches N_r	3
SNR	12 dB
SIR γ_{-1} [dB]	0, 10, 30, ∞
Channel	Raleigh fading + AWGN
Combining method	MMSE

4.2 BER Performances (with Interference)

In this subsection, we consider the effect of interference signals on the performance of the proposed diversity receiver with MMSE based interference cancellation method described in Sect. 3. We evaluate the performance on the following conditions.

- Single interference signal whose carrier frequency is at $f_c + f_s$ (See Fig. 8)
- Two interference signals whose carrier frequencies are at $f_c \pm f_s$ (See Fig. 3)

The simulation parameters used in this subsection are shown in Table 2. We assume the autocorrelation matrices in (26) are given as

$$R_{-1} = \mathrm{diag}\left(\left[1, 1, 0\right]^{\mathrm{T}}\right), \tag{33}$$

$$R_0 = I_{N_r} = I_3, \tag{34}$$

$$R_1 = \mathrm{diag}\left(\left[0, 1, 1\right]^{\mathrm{T}}\right). \tag{35}$$

First, we discuss the case of the single interference signal. A computer simulation of the performance of the proposed interference canceller using the system model shown in Fig. 4 for $s_{-1} = 0$ or $\gamma_{-1} \to \infty$ [26]. As mentioned above, the spectra of the input and output signals of the received antenna in this case are shown in Fig. 8. We assume that $\rho = 1$ and uniform distribution of the phase $U(2\pi)$.

The performances of the proposed MMSE based interference canceller for SIR γ_1 are shown in Fig. 9 in the case of single interference signal. We can see from the figure that BER performances are improved by increase in the number of arrival paths N_p, i.e., path diversity gain is obtained. When $\gamma_1 > 20$ dB, since noise components are dominant in terms of BER degradation, BER curves are saturated to MRC theory with $L = 2$ for $N_p = 2$ and that with $L = 3$ for $N_p > 8$. When $\gamma_1 > 10$ dB and $N_p > 2$, we gain improvement by the proposed canceller compared with MRC theory with $L = 2$ even if an interference signal caused by the effect of PVAP antenna contaminates the desired signal.

Then, we evaluate the BER performances of the proposed receiver in the case that two interference signals are at $f_c \pm f_s$ and show them in Fig. 10. The corresponding spectra and system model are shown in Fig. 3 and Fig. 4, respectively. The BER performances for SIR γ_1 are shown in Fig. 2 for $\gamma_{-1} = 0$, 10, and 30 dB. We set the number of arrival

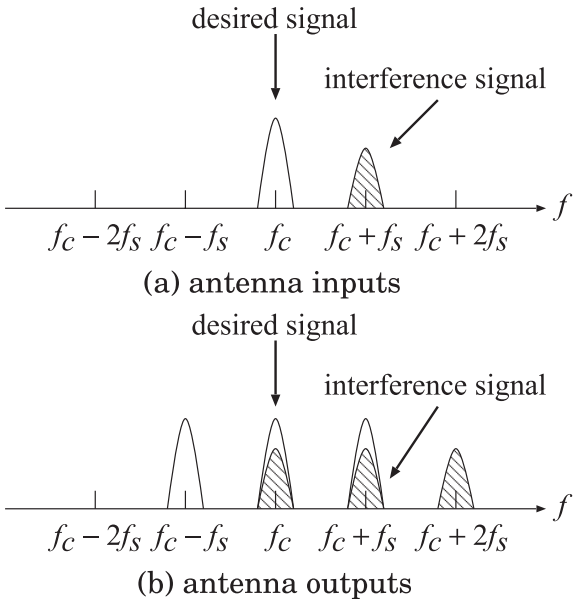

Fig. 8 Spectra of antenna input and output signals with an interference signal at $f_c + f_s$.

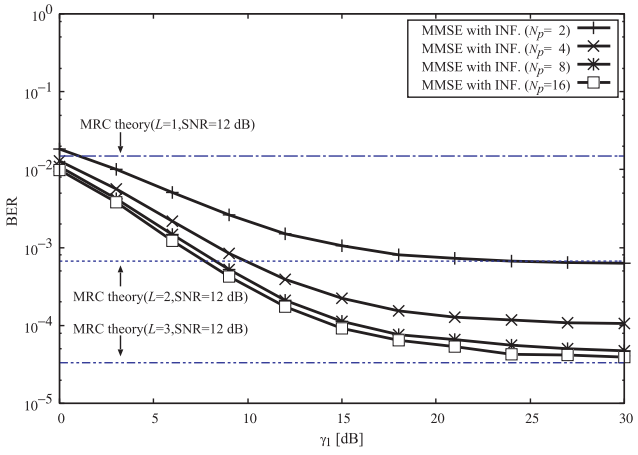

Fig. 9 BER performances obtained by the proposed MMSE based interference canceller with single interference signal at $f_c + f_s$.

paths as $N_p = 2, 16$.

The increase in SIR γ_1 improves the performances and then converges to a certain value of BER when $\gamma_1 > 20$ dB. When $\gamma_{-1} = 30$ dB, the performances are quite similar to those in Fig. 9, i.e., in the case of single interference signal. On the other hand, when $\gamma_{-1} = 0$ dB, it seems to be difficult to obtain diversity gain even if we use the interference canceller. In the case of $\gamma_{-1} = 10$ dB, we can see that the proposed canceller works well for both interference signals, in particular, in multipath rich environment due to path diversity. Similar to the case of single interference signal, the proposed MMSE based canceller improves the BER performances compared with MRC theory with $L = 2$.

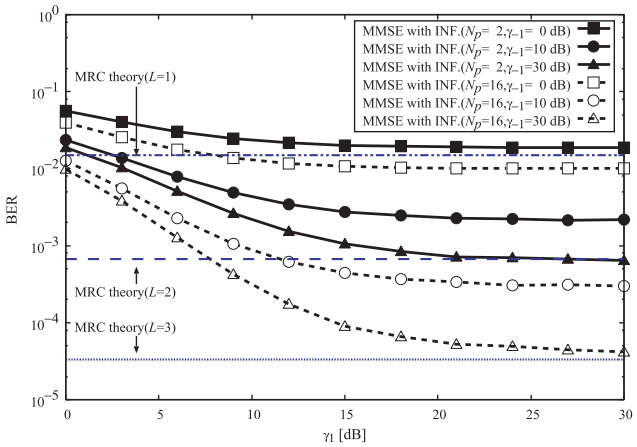

Fig. 10 BER performances obtained by the proposed MMSE based interference canceller with two interference signals at $f_c \pm f_s$ [27].

5. Conclusion

In this paper, we presented a diversity reception and interference cancellation for receivers using antenna with periodically variable antenna pattern. To evaluate the BER performances, we construct the system model considering the effect of the antenna pattern. Then, we propose an MMSE based interference canceller for the receiver.

We evaluate the BER of the receiver and confirm that path diversity gain can be obtained by the receiver. Also we confirm that the proposed interference canceller can achieve better BER performances than the conventional diversity receiver with two branches and MRC combiner without interference signals. Since the conventional receiver requires more antenna size than the proposed receiver, the proposed receiver can work well even if interference signals exist.

Future work can be the application of the proposed receiver model into Multiple-Input Multiple-Output (MIMO) systems to evaluate the capacity and BER performances of the system.

Acknowledgments

We would like to Y. Matsuda and M. Iimori for help with the study. A part of this work was supported by JSPS KAKENHI Grant Number 20K04468 and was carried out by the joint research program of the Institute of Materials and Systems for Sustainability, Nagoya University.

References

[1] Q. Yuan, M. Ishizu, Q. Chen, and K. Sawaya, "Modulated scattering array antenna for mobile handset," IEICE Electron. Express, vol.2, no.20, pp.519–522, Oct. 2005.
[2] Q. Chen, Y. Takeda, Q. Yuan, and K. Sawaya, "Diversity performance of modulated scattering array antenna," IEICE Electron. Express, vol.4, no.7, pp.216–220, April 2007.
[3] L. Wang, Q. Chen, Q. Yuan, and K. Sawaya, "Diversity performance of modulated scattering antenna array with switched reflector," IEICE Electron. Express, vol.7, no.10, pp.728–731, 2010.

[4] L. Wang, Q. Chen, Q. Yuan, and K. Sawaya, "Numerical analysis on MIMO performance of the modulated scattering antenna array in indoor environment," IEICE Trans. Commun., vol.E94-B, no.6, pp.1752–1756, June 2011.
[5] R. Bains and R. Muller, "Using parasitic elements for implementing the rotating antenna for MIMO receivers," IEEE Trans. Wireless Commun., vol.7, no.11, pp.4522–4533, 2008.
[6] S. Tsukamoto and M. Okada, "Single-RF diversity receiver for OFDM system using ESPAR antenna with alternate direction," ECTI Trans. Comput. and Inf. Technol., vol.6, no.1, pp.89–93, May 2012.
[7] D.J.R. Chisaguano, Y. Hou, T. Higashino, and M. Okada, "Low-complexity channel estimation and detection for mimo-ofdm receiver with espar antenna," IEEE Trans. Veh. Technol., vol.65, no.10, pp.8297–8308, 2016.
[8] K. Kawano and M. Saito, "Periodic reactance time functions for 2-element ESPAR antennas applied to 2-output SIMO/MIMO receivers," IEICE Trans. Commun., vol.E102-B, no.4, pp.930–939, April 2018. DOI: 10.1587/transcom.2018EBP3097.
[9] M. Saito, "Antenna pattern multiplexing for enhancing path diversity," Advances in Array Optimization, E. Aksoy, ed., ch. 4, IntechOpen, London, 2020. DOI: 10.5772/intechopen.89098.
[10] H. Kawakami and T. Ohira, "Electrically steerable passive array radiator (ESPAR) antennas," IEEE Antennas Propag. Mag., vol.47, no.2, pp.43–50, April 2005. DOI: 10.1109/MAP.2005.1487777.
[11] M. Saito, "A study on 4-output receive antenna by 2-element array antenna," Proc. CS Conf. IEICE'18, B-1-162, p.167, Sept. 2019.
[12] M. Saito, "A study on achieving multiple outputs of 3-element espar antenna by aliasing," Proc. CS Conf. IEICE'19, B-1-113, p.113, Sept. 2019.
[13] M. Saito, "Studies on receive diversity and mimo receivers based on the antenna with periodically variable antenna pattern," IEICE Technical Report, p.165, 2016.
[14] D.J.R. Chisaguano, Y. Hou, T. Higashino, and M. Okada, "Low-complexity channel estimation and detection for mimo-ofdm receiver with espar antenna," IEEE Trans. Veh. Technol., vol.65, no.10, pp.8297–8308, 2016.
[15] T. Ohira and K. Gyoda, "Electronically steerable passive array radiator antennas for low-cost analog adaptive beamforming," Phased Array Systems and Technology, 2000. Proceedings. 2000 IEEE International Conference on, pp.101–104, IEEE, 2000.
[16] Y. Idoguchi and M. Saito, "Evaluation of antenna with periodically variable directivity," Proc. 2014 Asia-Pacific Microwave Conference, pp.345–347, Nov. 2014.
[17] Q. Yuan, M. Ishizu, Q. Chen, and K. Sawaya, "Modulated scattering array antennas for mobile handsets," IEICE Electron. Express, vol.2, no.20, pp.519–522, 2005.
[18] K. Mitsuyama and N. Iai, "MMSE macrodiversity reception system with MER weighting method," J. ITE, vol.68, no.5, pp.J178–J183, 2014. DOI: 10.3169/itej.68.J178.
[19] H. Suzuki, "Interference cancelling characteristics of diversity reception with least-squares combining — MMSE characteristics and BER performance —," IEICE Trans. Commun. (Japanese Edition), vol.J74-B-II, no.12, pp.637–645, Dec. 1991.
[20] Y. Kamiya, Digital Wireless Communication Technologies with MATLAB, Corona Publishing, Tokyo, 2008.
[21] F. Maehara, "Significance of theoretical analysis in wireless system and its fascination," IEICE ESS Fundamentals Review, vol.7, no.1, pp.66–71, July 2013. DOI: 10.1587/essfr.7.60.
[22] T. Kobayashi, Wireless Communications by Andrea Goldsmith, MARUZEN-YUSHODO, Tokyo, 2007.
[23] H. Kawakami and T. Ohira, "Electrically steerable passive array radiator (ESPAR) antennas," IEEE Antennas Propag. Mag., vol.47, no.2, pp.43–50, April 2005.
[24] H. Tomoda, K. Kawano, and M. Saito, "A study on reactance time sequence for 2-element antenna with periodically variable antenna pattern," Proc. 2017 International Symposium on Antennas and Propagation (ISAP2017), Oct. 2017. DOI: 10.1109/ISANP.2017.8228963.
[25] N. Kinjo and M. Saito, "A study on antenna coefficient for diversity receivers using antenna with periodically variable antenna pattern," Proc. The 25th IEICE Kyushu Sec. Gakuseikai, A-25, Sept. 2017.
[26] M. Saito, "On interference cancellation of diversity receiver with periodically variable antenna pattern," Proc. ESS Conf. IEICE'16, A-9-9, p.128, Sept. 2016.
[27] N. Kinjo and M. Saito, "A study on MMSE based interference cancellation for diversity receivers using antenna with periodically variable antenna pattern," Proc. 70th Joint Conf. of Electrical, Electronics and Information Engineers in Kyushu, p.530, Sept. 2017.
[28] N. Goto, M. Nakagawa, and K. Ito, Antennas and Wireless Communication Handbook, Ohmsha, 2006.

Appendix: Derivation of (26)

In this section, we derive the weight (26) by minimizing the objective function J (25).

First, we rewrite (17) as

$$\begin{aligned}\boldsymbol{y} &= D_{-1}\boldsymbol{h}_{-1}\frac{s_{-1}}{\sqrt{\gamma_{-1}}} + D_0\boldsymbol{h}_0 s_0 + D_1\boldsymbol{h}_1\frac{s_1}{\sqrt{\gamma_1}} + \boldsymbol{n} \\ &= \boldsymbol{g}_{-1}\frac{s_{-1}}{\sqrt{\gamma_{-1}}} + \boldsymbol{g}_0 s_0 + \boldsymbol{g}_1\frac{s_1}{\sqrt{\gamma_1}} + \boldsymbol{n}, \end{aligned} \tag{A·1}$$

where $\boldsymbol{g}_k = D_k\boldsymbol{h}_k$ for $k = -1, 0, 1$.

The objective function J (25) can be expanded to

$$\begin{aligned} J &= \mathrm{E}\left[|z - s_0|^2\right] \\ &= \mathrm{E}\left[\left|\boldsymbol{w}^{\mathrm{H}}\boldsymbol{y} - s_0\right|^2\right] \\ &= \mathrm{E}\left[\left(\boldsymbol{w}^{\mathrm{H}}\boldsymbol{y} - s_0\right)\left(\boldsymbol{w}^{\mathrm{H}}\boldsymbol{y} - s_0\right)^*\right] \\ &= \mathrm{E}\left[\boldsymbol{w}^{\mathrm{H}}\boldsymbol{y}\left(\boldsymbol{w}^{\mathrm{H}}\boldsymbol{y}\right)^* - \boldsymbol{w}^{\mathrm{H}}\boldsymbol{y}s_0^* - \left(\boldsymbol{w}^{\mathrm{H}}\boldsymbol{y}\right)^* s_0 + |s_0|^2\right] \\ &= \mathrm{E}\left[\boldsymbol{w}^{\mathrm{H}}\boldsymbol{y}\boldsymbol{y}^{\mathrm{H}}\boldsymbol{w}\right] - \mathrm{E}\left[\boldsymbol{w}^{\mathrm{H}}\boldsymbol{y}s_0^*\right] - \mathrm{E}\left[\boldsymbol{y}^{\mathrm{H}}\boldsymbol{w}s_0\right] + 1 \\ &= \boldsymbol{w}^{\mathrm{H}}\mathrm{E}\left[\boldsymbol{y}\boldsymbol{y}^{\mathrm{H}}\right]\boldsymbol{w} - \boldsymbol{w}^{\mathrm{H}}\mathrm{E}\left[\boldsymbol{y}s_0^*\right] - \mathrm{E}\left[\boldsymbol{y}^{\mathrm{H}}s_0\right]\boldsymbol{w} + 1, \end{aligned} \tag{A·2}$$

where $\boldsymbol{w}$ can be outside of expectation because the weight vector is constant. In the first term of the right-hand side of (A·2), the autocorrelation matrix of $\boldsymbol{y}$ can be expanded to

$$\begin{aligned} &\mathrm{E}\left[\boldsymbol{y}\boldsymbol{y}^{\mathrm{H}}\right] \\ &= \mathrm{E}\left[\left(\boldsymbol{g}_{-1}\frac{s_{-1}}{\sqrt{\gamma_{-1}}} + \boldsymbol{g}_0 s_0 + \boldsymbol{g}_1\frac{s_1}{\sqrt{\gamma_1}} + \boldsymbol{n}\right)\right. \\ &\qquad \left.\left(\boldsymbol{g}_{-1}\frac{s_{-1}}{\sqrt{\gamma_{-1}}} + \boldsymbol{g}_0 s_0 + \boldsymbol{g}_1\frac{s_1}{\sqrt{\gamma_1}} + \boldsymbol{n}\right)^*\right] \\ &= \mathrm{E}\left[\boldsymbol{g}_{-1}\boldsymbol{g}_{-1}^{\mathrm{H}}\frac{|s_{-1}|^2}{\gamma_{-1}} + \boldsymbol{g}_{-1}\boldsymbol{g}_0^{\mathrm{H}}\frac{s_{-1}s_0^*}{\sqrt{\gamma_{-1}}} + \boldsymbol{g}_{-1}\boldsymbol{g}_1^{\mathrm{H}}\frac{s_{-1}s_1^*}{\sqrt{\gamma_{-1}\gamma_1}}\right. \\ &\qquad + \boldsymbol{g}_{-1}\boldsymbol{n}^{\mathrm{H}}\frac{s_{-1}}{\sqrt{\gamma_{-1}}} + \boldsymbol{g}_0\boldsymbol{g}_{-1}^{\mathrm{H}}\frac{s_0 s_{-1}^*}{\sqrt{\gamma_{-1}}} + \boldsymbol{g}_0\boldsymbol{g}_0^{\mathrm{H}}|s_0|^2 \\ &\qquad + \boldsymbol{g}_0\boldsymbol{g}_1^{\mathrm{H}}\frac{s_0 s_1^*}{\sqrt{\gamma_1}} + \boldsymbol{g}_0\boldsymbol{n}^{\mathrm{H}}s_0 + \boldsymbol{g}_1\boldsymbol{g}_{-1}^{\mathrm{H}}\frac{s_1 s_{-1}^*}{\sqrt{\gamma_1\gamma_{-1}}} \\ &\qquad \left.+\boldsymbol{g}_1\boldsymbol{g}_0^{\mathrm{H}}\frac{s_1 s_0^*}{\sqrt{\gamma_1}} + \boldsymbol{g}_1\boldsymbol{g}_1^{\mathrm{H}}\frac{|s_1|^2}{\gamma_1} + \boldsymbol{g}_1\boldsymbol{n}^{\mathrm{H}}\frac{s_1}{\sqrt{\gamma_1}}\right. \end{aligned}$$

$$+ \boldsymbol{n}\boldsymbol{g}_{-1}^{\mathrm{H}} \frac{s_{-1}^*}{\sqrt{\gamma_{-1}}} + \boldsymbol{n}\boldsymbol{g}_0^{\mathrm{H}} s_0^* + \boldsymbol{n}\boldsymbol{g}_1^{\mathrm{H}} \frac{s_1^*}{\sqrt{\gamma_1}} + \boldsymbol{n}\boldsymbol{n}^{\mathrm{H}}\Big]$$
$$= \frac{1}{\gamma_{-1}} \mathrm{E}\left[\boldsymbol{g}_{-1}\boldsymbol{g}_{-1}^{\mathrm{H}}\right] + \mathrm{E}\left[\boldsymbol{g}_0\boldsymbol{g}_0^{\mathrm{H}}\right] + \frac{1}{\gamma_1}\mathrm{E}\left[\boldsymbol{g}_1\boldsymbol{g}_1^{\mathrm{H}}\right] + \mathrm{E}\left[\boldsymbol{n}\boldsymbol{n}^{\mathrm{H}}\right]$$
$$= \frac{1}{\gamma_{-1}} R_{-1} + R_0 + \frac{1}{\gamma_1} R_1 + 2\sigma^2 I_{N_r}. \quad (\mathrm{A}\cdot 3)$$

The second term of the right-hand side of (A· 2) except for the constant weight vector is shown as

$$\mathrm{E}\left[\boldsymbol{y}s_0^*\right] = \mathrm{E}\left[\boldsymbol{g}_{-1}\frac{s_{-1}s_0^*}{\sqrt{\gamma_{-1}}} + \boldsymbol{g}_0|s_0|^2 + \boldsymbol{g}_1\frac{s_1 s_0^*}{\sqrt{\gamma_1}} + \boldsymbol{n}s_0^*\right]$$
$$= \mathrm{E}\left[\boldsymbol{g}_0\right], \quad (\mathrm{A}\cdot 4)$$

where the last term (A· 4) is referred to as cross-correlation vector between $D_0\boldsymbol{h}_0$ and s_0. In a similar manner, we have the third term of the right-hand side of (A· 2) except for $\boldsymbol{w}$ is

$$\mathrm{E}\left[\boldsymbol{y}^{\mathrm{H}}s_0\right] \quad (\mathrm{A}\cdot 5)$$

Thus, the object function J can be rewritten as

$$J = \boldsymbol{w}^{\mathrm{H}}\mathrm{E}\left[\boldsymbol{y}\boldsymbol{y}^{\mathrm{H}}\right]\boldsymbol{w} - \boldsymbol{w}^{\mathrm{H}}\mathrm{E}\left[\boldsymbol{g}_0\right] - \mathrm{E}\left[\boldsymbol{g}_0^{\mathrm{H}}\right]\boldsymbol{w} + 1. \quad (\mathrm{A}\cdot 6)$$

The weight vector $\boldsymbol{w}$ which minimizes J can be obtained by differentiating (A· 6) by $\boldsymbol{w}$ and equalizing it to a zero vector as follows [19], [28].

$$\frac{\partial J}{\partial \boldsymbol{w}} = 2\boldsymbol{w}^{\mathrm{H}}\mathrm{E}\left[\boldsymbol{y}\boldsymbol{y}^{\mathrm{H}}\right] - 2\mathrm{E}\left[\boldsymbol{g}_0^{\mathrm{H}}\right] = \boldsymbol{0} \quad (\mathrm{A}\cdot 7)$$

Then, we have

$$\boldsymbol{w}^{\mathrm{H}}\mathrm{E}\left[\boldsymbol{y}\boldsymbol{y}^{\mathrm{H}}\right] = \mathrm{E}\left[\boldsymbol{g}_0^{\mathrm{H}}\right]. \quad (\mathrm{A}\cdot 8)$$

Substituting (A· 3) into (A· 8) gives

$$\boldsymbol{w}^{\mathrm{H}}\left(\frac{1}{\gamma_{-1}}R_{-1} + R_0 + \frac{1}{\gamma_1}R_1 + 2\sigma^2 I_{N_r}\right) = \mathrm{E}\left[\boldsymbol{g}_0^{\mathrm{H}}\right]. \quad (\mathrm{A}\cdot 9)$$

The matrix in the left-hand side of (A· 9) has its inverse matrix. Then, right multiplying both sides of (A· 9) by the inverse matrix provides

$$\boldsymbol{w}^{\mathrm{H}} = \mathrm{E}\left[\boldsymbol{g}_0^{\mathrm{H}}\right]\left(\frac{1}{\gamma_{-1}}R_{-1} + R_0 + \frac{1}{\gamma_1}R_1 + 2\sigma^2 I_{N_r}\right)^{-1}. \quad (\mathrm{A}\cdot 10)$$

Taking Hermitian transpose of both sides of (A· 10), we have the weight vector as

$$\boldsymbol{w} = \left(\frac{1}{\gamma_{-1}}R_{-1} + R_0 + \frac{1}{\gamma_1}R_1 + 2\sigma^2 I_{N_r}\right)^{-1}\mathrm{E}\left[\boldsymbol{g}_0\right]$$
$$= \left(\frac{1}{\gamma_{-1}}R_{-1} + R_0 + \frac{1}{\gamma_1}R_1 + 2\sigma^2 I_{N_r}\right)^{-1}\mathrm{E}\left[D_0\boldsymbol{h}_0\right]. \quad (\mathrm{A}\cdot 11)$$

Nobuhide Kinjo received the B.E. and M.E. in Electrical and Electronics Engineering from University of the Ryukyus, Japan in 2017 and 2019, respectively. From 2019, he is with Radio Okinawa, Okinawa, Japan.

Masato Saito received the B.S., M.S., and Ph.D. degrees from Nagoya University, Aichi, Japan, in 1996, 1998, and 2001, respectively, all in Information Electronics Engineering. He was an Assistant Professor with Nara Institute of Science and Technology (NAIST), Nara, Japan, from 2001 to 2010. Since 2010, he has been an Associate Professor with University of the Ryukyus, Okinawa, Japan. From April 2007 to March 2008, he was a Visiting Researcher at ARC Special Research Centre for Ultra-Broadband Information Networks (CUBIN), the University of Melbourne, Melbourne, Australia. His research interests include wireless communications, satellite communications, and multi-hop networks. He is a member of IEEE.